JCTC Journal of Chemical Theory and Computation

Article

pubs.acs.org/JCTC

A Polarizable Force-Field for Cholesterol and Sphingomyelin

David Robinson*

School of Chemistry, University of Nottingham, University Park, Nottingham, NG7 2RD, United Kingdom

Supporting Information

ABSTRACT: A polarizable force-field, based on the Drude oscillator model, has been developed for cholesterol and the sphingomyelin class of lipids crucial to membrane raft formation, with testing performed on several 100 ns simulations. These have been validated against experimental observables as well as previous, nonpolarizable force-fields. Membrane bilayer properties, such as area-per-lipid and membrane thickness, produce results of comparable quantitative accuracy to those from the nonpolarizable force-field, while the membrane dipole potential is computed to be approximately 260 mV for a pure sphingomyelin bilayer, showing quantitative agreement with experimental results.

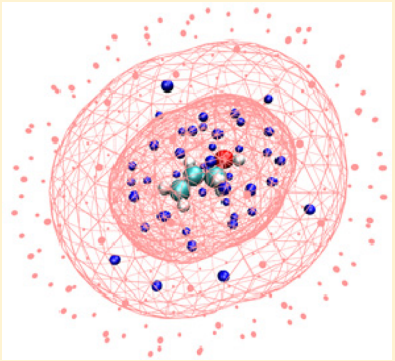

INTRODUCTION

During the past two decades, molecular dynamics simulations of phospholipid membrane systems have been performed with increasing numbers of atoms and ever longer time scales. Woolf and Roux[1] demonstrated that the boundary between lipid headgroups and bulk solvent was much broader than previously thought, highlighting the utility of combined theoretical and experimental approaches. An explicit characterization of the nature of intermolecular interactions between the gramicidin A channel (protein) and the membrane was possible: tryptophan residues located on the interface between the protein and membrane hydrogen bond to the ester carbonyl group of the membrane lipids, suggesting the important contribution of such interactions in stabilizing membrane proteins. More recently, several studies have determined properties of membranes and transmembrane proteins with atomistic detail. The structure and mechanism of the Na+/H+ antiporter (*Escherichia coli* NhaA) in lipid membranes was determined,[2] complementing previous experimental investigations.[3]

The formation of transient membrane defects was studied by Vattulainen et al., giving insights into defect-mediated trafficking across membranes with a resolution unattainable by current experimental methods.[4] Studies of membrane domains with high-cholesterol concentrations have been performed by several groups.[5−9] These regions are often referred to as rafts; these are considered important in cellular signaling, although experimental evidence in vitro is very difficult to attain.[10] Membrane rafts are a current area of intense study, and a definitive description of what constitutes a raft is still a matter of debate. However, many studies agree that raft domains are regions of lipid membranes in which there is an enhanced concentration of sphingolipids and cholesterol with respect to nonraft regions, and these components are found to pack more tightly than in the surrounding membrane, giving rise to a liquid-ordered (l_o) region, which coexist with the surrounding nonraft, liquid-disordered (l_d) regions. The origin of the tighter packing has been speculated to be hydrogen-bonding between the sphingolipids and cholesterol, or stronger van der Waals' interactions between the sphingolipids and cholesterol than is for found for other classes of lipids (e.g., DPPC);[8] describing such packing using molecular dynamics requires polarization effects to be included both for qualitative and quantitative accuracy. Further interest in sphingomyelin comes from its other roles within cell membranes: metabolic derivatives of sphingomyelin are involved in cell signaling, cell proliferation is mediated by sphingosine, and hydrolysis products of sphingomyelin act as secondary messengers for the stimulation of phosphatases and kinases, responsible for cell growth regulation and apoptosis.

The successive developments of membrane force-fields have led to the CHARMM36 lipid force-field, which for many properties are predicted with quantitative accuracy.[11] However, one of the main properties, the membrane dipole potential, is known to be incorrectly predicted unless some form of polarization is included within the force-field. The non-polarizable force-fields attempt to capture many-body polarization effects in an averaged way, using partial atomic charges that are invariant to their electrostatic environment. To this end, there has been some effort recently to introduce polarizable force-fields for the various lipids found in cell membranes,[12−14] although there still remains only a non-polarizable force-field for the sphingomyelin molecules[15] and cholesterol.[16,17]

Received: February 8, 2013
Published: April 4, 2013

COMPUTATIONAL DETAILS

I. Charge Fitting. For the polarizable force-field, we employ the Drude oscillator model, as implemented in the CHARMM[18−20] and NAMD[21,21] packages. In this method, a massless particle is attached to each polarizable atom with a harmonic spring. A finite induced dipole is created, with the partial atomic charge redistributed between the polarizable atom and the Drude particle. In practice, the partial atomic charge is given as

$$q = q_a + q_D \tag{1}$$

where q_a is the charge on the polarizable atom core and q_D is the charge on the Drude particle. The polarizability for a given atom is related to the charge on the Drude particle via eq 2

$$\alpha = \frac{q_D^2}{k_D} \tag{2}$$

where k_D is the force constant for the harmonic spring connecting the Drude particle to the polarizable atom core.

The electrostatic energy term for the Drude polarizable force-field is modified to give

$$U_{elec} = \sum_{A<B}^{N} \frac{q_a(A)\cdot q_a(B)}{|r(A) - r(B)|} + \sum_{A<B}^{N,N_D} \frac{q_D(A)\cdot q_a(B)}{|r_D(A) - r(B)|} + \sum_{A<B}^{N_D} \frac{q_D(A)\cdot q_D(B)}{|r_D(A) - r_D(B)|} + \frac{1}{2}\sum_{A}^{N_D} k_D |r_D(A) - r(A)|^2 \tag{3}$$

where the pairwise additive potential is described by interactions of the atomic cores and the Drude particles and the harmonic term gives the self-energy of a polarizable atom.

The charge-fitting scheme follows the protocol of MacKerrell et al.,[23] and the reader is referred to this reference for full details of the fitting scheme. Geometries of small molecule analogues of sphingomyelin are obtained at the MP2/6-31G(d) level of theory (see Supporting Information). The relative spacing of the Connolly surfaces, as well as the density of grid points, are given in Table 1. For the ceramide linkage, this scheme gave a total of 43 perturbation charges and 1621 ESP grid points; Figure 1 represents the placing of the perturbation charges around the lone pairs. Similar values for the model compounds used for cholesterol can be found in the Supporting Information. Quantum mechanical calculations are performed on the molecule of interest with one perturbation charge at a time, using the Q-Chem software package.[24] The B3LYP density functional[25] is chosen, along with the aug-cc-pVDZ basis set of Dunning[26] for the calculation of the ESP maps. Partial atomic charges are then generated by use of the restrained ESP (RESP) fitting scheme, yielding the following equation:

$$\chi_r^2 = \sum_{A}^{N} \{w[q(A) - \bar{q}(A)]^2 + w_D[q_D(A) - \bar{q}_D(A)]^2\} \tag{4}$$

where $\bar{q}$ and $\bar{q}_D$ are reference values (initial values) for the atomic and Drude charges, respectively. Initial estimates for the partial charges of the atoms and Drude particles were taken (where possible) from the polarizable force-field for DPPC,[12] corresponding to $\bar{q}(A)$ and $\bar{q}_D(A)$ in eq 4. Other values, for atomic species not present in ref 12, were taken from similar molecules already parametrized with the Drude force-field. The value of the atom-Drude force-constant, k_D, was fixed at 500 kcal mol^{-1} Å^{-2}, consistent with other molecules parametrized with the Drude force-field, thus allowing the RESP procedure to be applied only to the partial charges. Clearly, the initial values of the partial atomic charges need to be a good guess; otherwise the value of eq 4 will never converge. The optimized values for the partial atomic charges are given in the Supporting Information.

Geometric parameters for sphingomyelin and cholesterol were taken from previous works;[15−17] since the Drude model is a modification of only the electrostatic term, the geometric parameters are calculated in analogy with those found in the nonpolarizable force-field. Since these parameters already exist (and in modified form for the phosphatidylcholine headgroup and aliphatic chains[11]), then optimization of these parameters for these molecules is redundant. Lennard-Jones parameters were tested and readjusted to values consistent with those previously optimized using the Drude polarizable force-field for cyclo-alkanes.[27]

ii. Molecular Dynamics Simulations. For the pure sphingomyelin (SPEI) bilayer, 200 sphingomyelin (16:0) molecules (where the notation refers to 16 atoms on the "amide" lipid chain) and 10 000 SWM4 polarizable water molecules[28,29] were used, giving a total of 87 400 atomic sites (including Drude particles). The mixed SPEI/cholesterol (CHOL) bilayer had 140 SPEI molecules and 60 CHOL molecules, with 10 000 SWM4 water molecules (82 420 atomic sites, including Drude particles). Since polarizable integrators are poor at handling bad contacts, it is necessary to use a nonpolarizable force-field to obtain and initially stablilize a

Table 1. Parameters for the Charge and Grid Point Surface Generation for Model Compounds Studied

surface	size factor[a]	density factor
charges (1)	2.2	1.2
ESP grid 1	3.0	1.2
charges (2)	4.0	0.5
ESP grid 2	5.0	0.5
ESP grid 3	6.0	0.1

[a]The size factor is multiplied by the van der Waals radius of each atom in the molecule to generate the relevant Connolly surface.

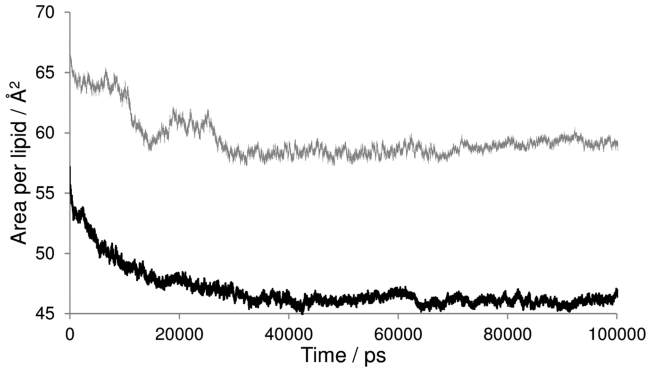

Figure 1. Evolution of the surface area per lipid for the two simulations, pure sphingomyelin (dashed line) and the mixed sphingomyelin/cholesterol bilayer (solid line), calculated at 321 K.

configuration. Thus, equilibration was done in two stages: the nonpolarizable system was equilibrated; then the Drude particles were added and equilibration reperformed with the polarizable model. SPEI molecules were mutated from pre-equilibrated dipalmitoylphosphatidylcholine (DPPC) lipid molecules, by replacing the glycol linkage with the sphingosine linkage. The system was first equilibrated using the non-polarizable force-field[30] as follows: TIP3P water[31] was used in place of SWM4 water. A total of 500 steps of steepest-descent minimization were initially used to remove any bad contacts, followed by a further 1000 steps of adapted basis Newton–Raphson (ABNR) minimization. Equilibration dynamics were performed initially using a 1 fs time step for 50 ps with a nonbond cutoff of 16 Å, with the force-based switching function starting at 10 Å and eliminating all pair contributions at 12 Å. Long-range electrostatics were treated using the Particle Mesh Ewald (PME) algorithm, using a sixth order spline interpolation.[32] Langevin temperature control was used, with damping of 10 ps^{-1}. Periodic boundary conditions were used, using tetragonal symmetry. A harmonic term was used to restrain the lipid headgroups from moving too far from their starting positions. The SHAKE algorithm[33] was used to constrain all bonds to hydrogen atoms. Further equilibration for 500 ps was performed using a 2 fs time step and a Langevin barostat with a piston period of 50 fs and a decay period of 25 fs, with the harmonic term removed. The final snapshot from this nonpolarizable equilibration was used as the starting point for the polarizable simulation. The residues had Drude particles added, and the above equilibration steps were used with the polarizable force-field, except that a 1 fs time step was used throughout, with the SHAKE/Roll[34] and RATTLE/Roll[35] algorithms being employed to constrain covalent bonds with hydrogen. A dual Langevin thermostat was used,[36] such that the Drude particles were kept at ∼1 K, while the real atoms were kept close to 321.15 K. This temperature was chosen since a bilayer consisting of spingomyelin lipids is found in the liquid-ordered state below this temperature. Equilibration lasted for 25 ns. Production dynamics were carried out with the same temperature and parameters, without the rescaling of velocities, for a further 75 ns. A further simulation was carried out, in which the temperature was gradually decreased to 310 K and equilibrated for 25 ns, with the other simulation details kept as above (for the mixed cholesterol/sphingomyelin system only). Production dynamics for this system (310 K) were carried out for a further 75 ns.

RESULTS AND DISCUSSION

To verify the new lipid parameters for sphingomyelin and cholesterol (given in the Supporting Information), comparison with experimental structural and dynamical parameters is necessary. Given in Figure 2 is the evolution of the surface area per lipid during the equilibration phase of the simulation. The area per lipid converges to a stable value of 58 $Å^2$ (with standard deviation, σ = 0.57 Å) for the pure sphingomyelin simulation and 46.5 $Å^2$ (σ = 0.27 Å) for the sphingomyelin/cholesterol simulation. Experimental estimates vary from 50 − 60 $Å^2$ and the experimental determination of this property is known to be difficult.[37] The experimental uncertainty is of the same magnitude as our computed values. No experimental or computed data exists for the mixed system at 321 K; the values computed using a simulation at 310 K using sphingomyelin (18:0) give a converged value of 46 $Å^2$, in agreement with a previous studies' value[38] of 44.5 $Å^2$. Presented in Figure 3 are

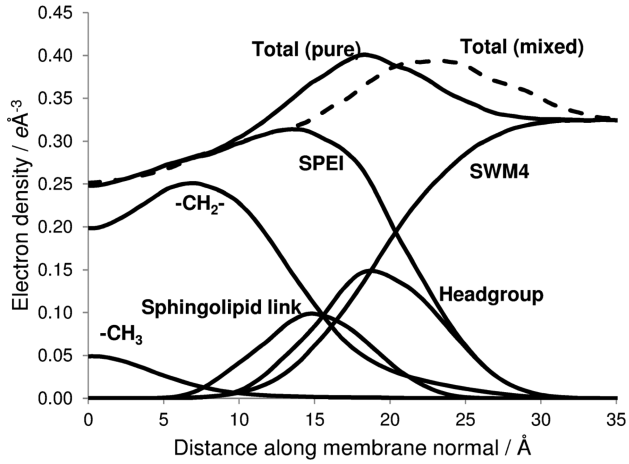

Figure 2. Computed total electron density profiles for the pure sphingomyelin bilayer (labeled "Total (pure)") and for the mixed bilayer (labeled "Total (mixed)"), calculated at 321 K. The contribution to the total electron density for sphingomyelin from different topological groups is also given.

the electron density profiles calculated for the two systems of interest. For the pure sphingomyelin system, the bilayer thickness is computed to be 36.4 Å (±0.5 Å), in good agreement with the experimental value[37] of 36.5 Å (±0.5 Å). The mixed system has a bilayer thickness of 42.6 Å, again in good agreement with experiment.[39] The uncertainty in the simulations and experiment is essentially the same for the membrane thickness. The contribution to the total electron density is very similar to that shown for the nonpolarizable force-field.[30] The electron densities calculated over the first 5 ns of production dynamics and the last 5 ns of production dynamics show very little difference, indicating a well equilibrated system used for production dynamics (see Supporting Information).

The membrane dipole potential is the key value for which nonpolarizable force-fields of lipids fail to give quantitative accuracy, although relative qualitative accuracy is achieved. The correct dipole potential was achieved with the Drude polarizable force-field for DPPC,[12] on which the current sphingomyelin parameters are based. The membrane dipole potential profile was calculated as the double integral of the charge density, given in eq 5.

$$\phi(z) - \phi(0) = -\frac{1}{\varepsilon_0}\int_0^z \mathrm{d}z' \int_0^{z'} \mathrm{d}z''\rho_c(z'') \quad (5)$$

following Feller et al.[40] The membrane dipole potential was calculated to be ∼260 mV in the pure sphingomyelin system (321 K), in good agreement with the experimental estimate for lipids with phosphatidylcholine (PC) headroups (∼300 mV). An increase of ∼110 mV was found in the dipole potential when a 30 mol % concentration of cholesterol was added, agreeing quantitatively with experimental studies of membrane bilayers containing lipids with phosphatidylcholine head-groups.[41] A similar difference in dipole potential was observed at 310 K, although the absolute dipole potentials were ∼60 mV higher than those calculated at 321 K.

The lateral diffusion coefficients were calculated using the Einstein relation, with the method employed in CHARMM described in the literature[42]

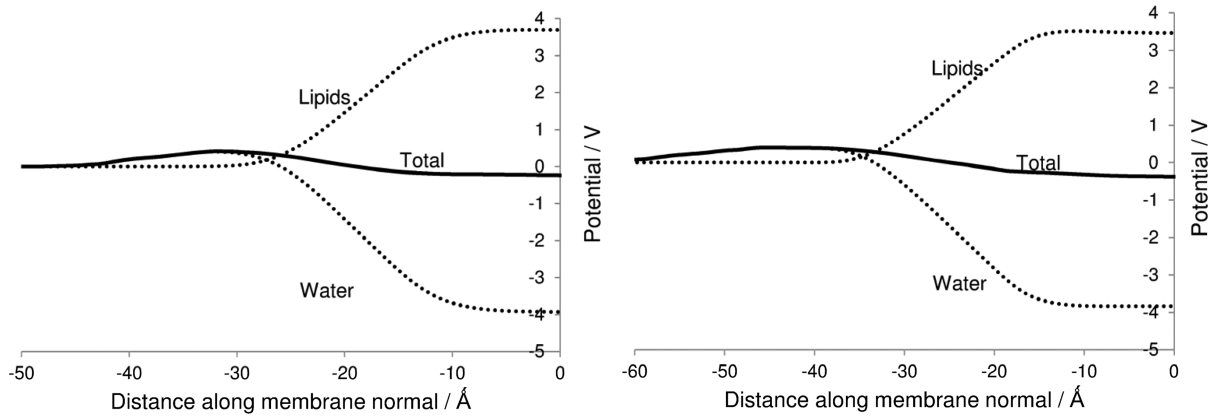

Figure 3. Computed electrostatic potential profiles (left-hand side, pure sphingomyelin bilayer; right-hand side, mixed sphingomyelin/cholesterol bilayer).

$$D(t) = \lim_{t\to\infty} \frac{\langle r^2(t)\rangle}{4t} \tag{6}$$

where $\langle r^2(t)\rangle$ represents the measure mean-squared (MSD) displacement of the lipids. The calculated values of 0.55 Å^2 ns^{-1} and 0.30 Å^2 ns^{-1} are in good agreement with the experimentally determined values of 0.6 Å^2 ns^{-1} and ∼0.28 Å^2 ns^{-1}.[43] Pastor et al. demonstrated that for membrane systems with a box size of ∼50 Å or less, the calculated values of the lateral diffusion coefficients were affected by the PME method and that this problem manifested itself in the calculated MSD of the individual leaflets; the box size of the membranes considered in the current work is substantially larger (∼80 Å in the x and y directions), and the MSDs for the individual (entire) leaflets are close to zero, so we can conclude that the finite-size problem is not an issue with the current simulations. Another useful structural parameter commonly used is the deuterium order parameters, experimentally determined from NMR experiments

$$S_{CD} = \frac{1}{2}\langle 3\cos^2\theta - 1\rangle \tag{7}$$

The computed order parameters are shown in Figure 4, along with experimental data and estimates of the associated uncertainties. The values computed at 321 K compare well with experimentally determined values,[44,45] within the uncertainty reported. Experimental results for the order parameter at 310 K are, to the best knowledge of the author, unavailable, and so we compare the parameters calculated at 310 K with those from the previous nonpolarizable force-field;[15] again, these compare well. As expected for these lipid types, addition of cholesterol increases the order parameters (data not shown). Radial distribution functions (RDF) between carbon atoms at the same chain position of spingomyelin for the membrane bilayers confirm an increase in packing of lipids in the mixed system compared with the packing found in the pure bilayer (see Supporting Information). Figure 5 shows the RDF

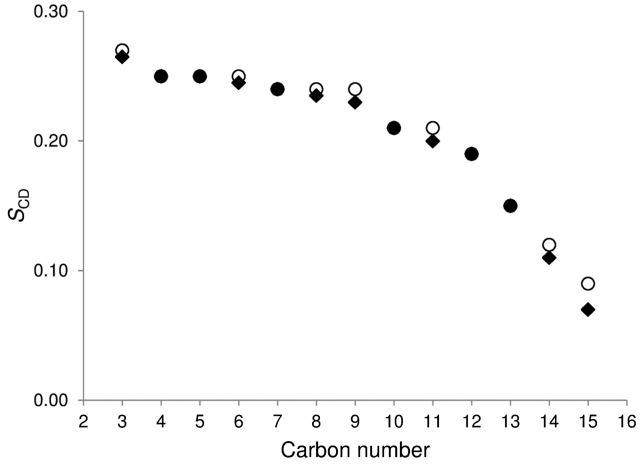

Figure 4. Computed deuterium order parameters (321 K) for sphingomyelin: computed (diamonds) and experimental: (circles) from ref 43.

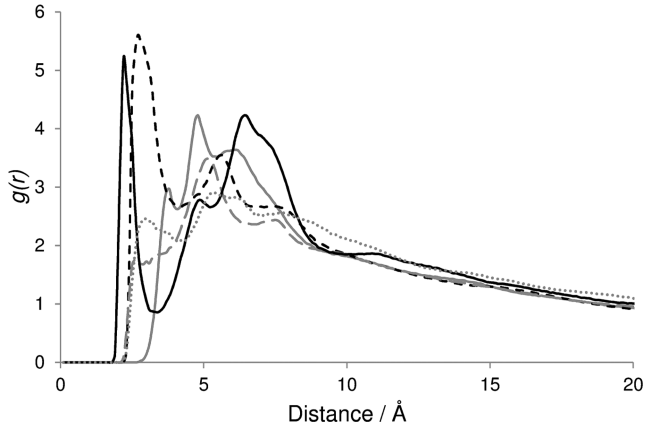

Figure 5. Radial distribution functions between pairs of hydrogen bond donors/acceptors of the sphingomyelin (SPEI) and cholesterol (CHOL) molecules, calculated at 321 K. SPEI O3 − CHOL H3′ (light gray dashes), SPEI N21 − CHOL H3′ (solid light gray), SPEI O22 − CHOL H3′ (long dashes), CHOL O3 − SPEI HN (solid line), CHOL O3 − SPEI HO (light gray dots). Atom types refer to the CHARMM topological atom types (see Supporting Information).

between the hydrogen bond donors and acceptors of sphingomyelin and cholesterol. Peaks in the RDFs corresponding to hydrogen bond distances between 2.2 Å and 2.8 Å are observed between the hydrogen bond donors of sphingomyelin and the −OH oxygen of cholesterol, and also between the carbonyl oxygen of sphingomyelin and the −OH hydrogen of cholesterol. The hydrogen bond between the −OH oxygen of cholesterol and the hydrogen of the −NH group of sphingomyelin is particularly important, since this bond does not exist for other classes of lipid, such as DPPC. At 310 K,

dx.doi.org/10.1021/ct400103e | J. Chem. Theory Comput. 2013, 9, 2498−2503

these peaks increase in size, showing that hydrogen bonding between sphingomyelin and cholesterol is important in the formation of the liquid-ordered phase.[46]

Using the Drude model for polarizability allows one to explicitly calculate the point dipole that is induced in one molecule due to the presence of a second molecule. In a situation where the difference between the relaxed dipole moment and the calculated dipole moment incorporating the effect of polarization is small, then a nonpolarizable force-field is suitable for use for the calculation of electrostatic effects. Figure 6 presents the calculated dipole moments from the

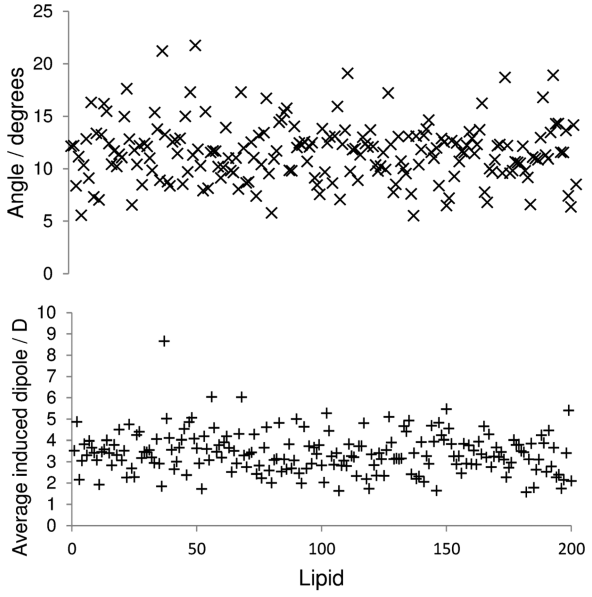

Figure 6. (i) Average angle change due to induced dipole of sphingomyelin (top). (ii) Average induced dipole (bottom), calculated at 321 K.

simulations, along with the dipole moment when the Drude particles are allowed to relax. The average induced dipole for sphingomyelin is 3.41 D in the pure sphingomyelin system (3.4 D in the mixed system) and 0.5 D for cholesterol. The average change in the angle of the dipole moment with respect to the membrane normal is 11.6°. These values represent an induced dipole that is ∼10% of the total average dipole moment for a single lipid, and significant for cholesterol. It is clear that the polarizable force-field is therefore necessary to describe lipid−lipid and lipid−cholesterol interactions correctly. Presented in Figure 7 are the average dipole moments for water molecules over the course of the trajectory with respect to the distance along the membrane normal. Far from the headgroup, the dipole moment gives an average value of 2.38 D, close to the bulk water dipole moment of 2.45 D for the SWM4 model. Closer to the headgroup, the calculated dipole moment changes significantly due to polarization, ranging between 1.6 and 2.9 D. One must therefore use a polarizable model if the dielectric environment of the membrane bilayer is of importance, such as in studies of molecule trafficking across a membrane.

CONCLUSIONS

This work has considered the development of a polarizable force-field for the major components of membrane raft domains that is consistent with previous polarizable force-fields. The properties computed with the new force-field show

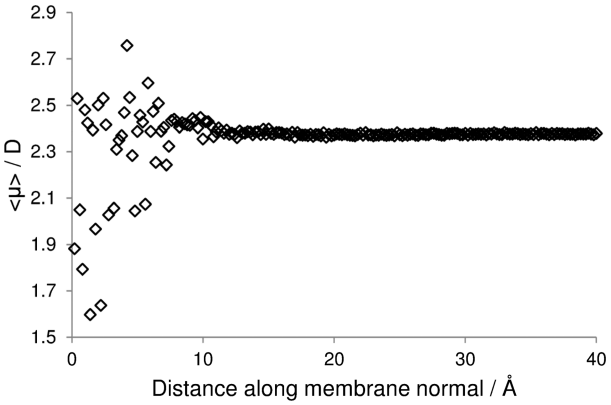

Figure 7. Trajectory averaged dipole moments for water molecules with respect to the distance along the membrane normal, calculated at 321 K.

good agreement with the available experimental data for a wide variety of properties and also represent an improvement over the nonpolarizable force-fields for properties such as the membrane dipole potential and induced dipole moments. Along with the SWM4 water molecule force-field and the DPPC force-field, it should be possible to perform simulations on membrane raft-like domains using the fully polarizable Drude oscillator model to give qualitative and quantitative agreement with experimental detail.

ASSOCIATED CONTENT

Supporting Information

CHARMM-compatible topology files, Lennard-Jones parameters, and small molecule parametrization data are available. This material is available free of charge via the Internet at http://pubs.acs.org.

AUTHOR INFORMATION

Corresponding Author

*E-mail: david.robinson@nottingham.ac.uk.

Notes

The authors declare no competing financial interest.

ACKNOWLEDGMENTS

I thank the University of Nottingham HPC service for provision of computer time. I thank the Leverhulme Trust for the award of an Early Career Fellowship. I also thank A. D. MacKerell and L. Huang for providing the FITCHARGE program for the fitting of atomic partial charges to the ESP maps.

REFERENCES

(1) Woolf, T. B.; Roux, B. *Proc. Natl. Acad. Sci. U. S. A.* **1994**, *91*, 11631−11635.
(2) Arkin, I. T.; Xu, H.; Jensen, M. Ø.; Arbely, E.; Bennett, E. R.; Bowers, K. J.; Chow, E.; Dror, R. O.; Eastwood, M. P.; Flitman-Tene, R.; Gregersen, B. A.; Klepeis, J. L.; Kolossváry, I.; Shan, Y.; Shaw, D. E. *Science* **2007**, *317*, 799−803.
(3) Hunte, C.; Screpanti, E.; Venturi, M.; Rimon, A.; Padan, E.; Michel, H. *Nature* **2005**, *435*, 1197−1202.
(4) Gurtovenko, A. A.; Anwar, J.; Vattulainen, I. *Chem. Rev.* **2010**, *110*, 6077−6103.
(5) Robinson, D.; Besley, N. A.; O'Shea, P.; Hirst, J. D. *J. Comput. Chem.* **2011**, *32*, 2613−2618.

(6) Mihailescu, M.; Vaswani, R. G.; Jardón-Valadez, E.; Castro-Román, F.; Freites, J. A.; ZWorcester, D. L.; Chamberlin, A. R.; Tobias, D. J.; White, S. H. *Biophys. J.* **2011**, *100*, 1455−1462.
(7) O'Connor, J. W.; Klauda, J. B. *J. Phys. Chem. B* **2011**, *115*, 6455−6464.
(8) Zidar, J.; Merzel, F.; Hodoscek, M.; Rebolj, K.; Sepcic, K.; Macek, P.; Janezic, D. *J. Phys. Chem. B* **2009**, *113*, 15795−15802.
(9) Simons, K.; Ikonen, E. *Nature* **1997**, *387*, 569−572.
(10) Simons, K.; Toomre, D. *Nat. Rev. Mol. Cell Biol.* **2000**, *1*, 31−39.
(11) Klauda, J. B.; Venable, R. M.; Freites, J. A.; O'Connor, J. W.; Tobias, D. J.; Mondragon-Ramirez, C.; Vorobyov, I.; MacKerell, A. D., Jr.; Pastor, R. W. *J. Phys. Chem. B* **2010**, *114*, 7830−7843.
(12) Harder, E.; MacKerell, A. D., Jr.; Roux, B. *J. Am. Chem. Soc.* **2009**, *131*, 2760−2761.
(13) Vorobyov, I.; Allen, T. W. *J. Chem. Phys.* **2010**, *132*, 185101.
(14) Bauer, B. A.; Lucas, T. R.; Meninger, D. J.; Patel, S. *Chem. Phys. Lett.* **2011**, *508*, 289−294.
(15) Hyvönen, M .T.; Kovanen, P. T. *J. Phys. Chem. B* **2003**, *107*, 9102−9108.
(16) Pitman, M. C.; Suits, F.; MacKerell, A. D., Jr.; Feller, S. E. *Biochemistry* **2004**, *43*, 15318−15328.
(17) Lim, J. B.; Rogaski, B.; Klauda, J. B. *J. Phys. Chem. B* **2012**, *116*, 203−210.
(18) Brooks, B. R.; Brooks, C. L., III; MacKerell, A. D., Jr.; Nilsson, L.; Petrella, R. J.; Roux, B.; Won, Y.; Archontis, G.; Bartels, C.; Boresch, S.; Caflisch, A.; Caves, L.; Cui, Q.; Dinner, A. R.; Feig, M.; Fischer, S.; Gao, J.; Hodoscek, M.; Im, W.; Kuczera, K.; Lazaridis, T.; Ma, J.; Ovchinnikov, V.; Paci, E.; Pastor, R. W.; Post, C. B.; Pu, J. Z.; Schaefer, M.; Tidor, B.; Venable, R. M.; Woodcock, H. L.; Wu, X.; Yang, W.; York, D. M.; Karplus, M. *J. Comput. Chem.* **2009**, *30*, 1545−1615.
(19) Lamoureux, G.; Roux, B. *J. Chem. Phys.* **2003**, *119*, 3025−3039.
(20) Harder, E.; Anisimov, V. M.; Vorobyov, I. V.; Lopes, P. E. M.; Noskov, S. Y.; MacKerell, A. D., Jr.; Roux, B. *J. Chem. Theory Comput.* **2006**, *2*, 1587−1597.
(21) Phillips, J. C.; Braun, R.; Wang, W.; Gumbart, J.; Tajkhorshid, E.; Villa, E.; Chipot, C.; Skeel, R. D.; Kale, L.; Schulten, K. *J. Comput. Chem.* **2005**, *26*, 1781−1802.
(22) Jiang, W.; Hardy, D. J.; Phillips, J. C.; MacKerell, A. D., Jr.; Schulten, K.; Roux, B. *J. Phys. Chem. Lett.* **2011**, *2*, 87−92.
(23) Anisimov, V. M.; Lamoureux, G.; Vorobyov, I. V.; Huang, N.; Roux, B.; MacKerell, A. D., Jr. *J. Chem. Theory Comput.* **2005**, *1*, 153−168.
(24) Shao, Y.; Molnar, L. F.; Jung, Y.; Kussmann, J.; Ochsenfeld, C.; Brown, S. T.; Gilbert, A. T. B.; Slipchenko, L. V.; Levchenko, S. V.; O'Neill, D. P.; DiStasio, R. A., Jr.; Lochan, R. C.; Wang, T.; Beran, G. J. O.; Besley, N. A.; Herbert, J. M.; Lin, C. Y.; Van Voorhis, T.; Chien, S. H.; Sodt, A.; Steele, R. P.; Rassolov, V. A.; Maslen, P. E.; Korambath, P. P.; Adamson, R. D.; Austin, B.; Baker, J.; Byrd, E. F. C.; Dachsel, H.; Doerksen, R. J.; Dreuw, A.; Dunietz, B. D.; Dutoi, A. D.; Furlani, T. R.; Gwaltney, S. R.; Heyden, A.; Hirata, S.; Hsu, C.-P.; Kedziora, G.; Khalliulin, R. Z.; Klunzinger, P.; Lee, A. M.; Lee, M. S.; Liang, W.; Lotan, I.; Nair, N.; Peters, B.; Proynov, E. I.; Pieniazek, P. A.; Rhee, Y. M.; Ritchie, J.; Rosta, E.; Sherrill, C. D.; Simmonett, A. C.; Subotnik, J. E.; Woodcock, H. L., III.; Zhang, W.; Bell, A. T.; Chakraborty, A. K.; Chipman, D. M.; Keil, Frerich, J.; Warshel, A.; Hehre, W. J.; Schaefer, H. F., III.; Kong, J.; Krylov, A. I.; Gill, P. M. W.; Head-Gordon, M. *Phys. Chem. Chem. Phys.* **2006**, *8*, 3172−3191.
(25) Becke, A. D. *J. Chem. Phys.* **1993**, *98*, 5648−5652.
(26) Dunning, T. H. *J. Chem. Phys.* **1989**, *90*, 1007−1023.
(27) Vorobyov, I. V.; Anisimov, V. M.; MacKerell, A. D., Jr. *J. Phys. Chem. B* **2005**, *109*, 18988−18999.
(28) Lamoureux, G.; MacKerell, A. D., Jr.; Roux, B. *J. Chem. Phys.* **2003**, *119*, 5185−5197.
(29) Lamoureux, G.; Harder, E.; Vorobyov, I. V.; Roux, B.; MacKerell, A. D., Jr. *Chem. Phys. Lett.* **2006**, *418*, 245−249.
(30) Hyvönen, M. T.; Kovanen, P. T. *J. Phys. Chem. B* **2003**, *107*, 9102−9108.
(31) Jorgensen, W. L.; Chandrasekhar, J.; Madura, D.; Impey, R. W.; Klein, M. L. *J. Chem. Phys.* **1983**, *79*, 926−935.
(32) Essmann, U.; Perera, L.; Berkowitz, M. L.; Darden, T.; Lee, H.; Pedersen, L. G. *J. Chem. Phys.* **1995**, *103*, 8577−8593.
(33) Ryckaert, J.-P.; Ciccotti, G.; Berendsen, H. J. C. *J. Comput. Phys.* **1977**, *23*, 327−341.
(34) Martyna, G. J.; Tuckerman, M. E.; Tobias, D. J.; Klein, M. L. *Mol. Phys.* **1996**, *87*, 1117−1157.
(35) Andersen, H. C. *J. Comput. Phys.* **1983**, *52*, 24−34.
(36) Lamoureux, G.; Roux, B. *J. Chem. Phys.* **2003**, *119*, 3025−3039.
(37) Ramstedt, B.; Slotte, J. P. *Biophys. J.* **1999**, *77*, 1498−1506.
(38) Khelashvili, G. A.; Scott, H. L. *J. Chem. Phys.* **2004**, *120*, 9841−9847.
(39) Maulik, P. R.; Sripada, P. K.; Shipley, G. G. *Biochim. Biophys. Acta* **1991**, *62*, 211−219.
(40) Feller, S. E.; Pastor, R. W.; Rojnuckarin, A.; Bogusz, S.; Brooks, B. R. *J. Phys. Chem.* **1996**, *100*, 17011−17020.
(41) Starke-Peterkovic, T.; Turner, N.; Vitha, M. F.; Waller, M. P.; Hibbs, D. E.; Clarke, R. J. *Biophys. J.* **2006**, *90*, 4060−4070.
(42) Klauda, J. B.; Brooks, B. R.; Pastor, R. W. *J. Chem. Phys.* **2006**, *125*, 144710.
(43) Filippov, A.; Oradd, G.; Lindblom, G. *Biophys. J.* **2003**, *84*, 3079−3086.
(44) Mehnert, T.; Jacob, K.; Bittman, R.; Beyer, K. *Biophys. J.* **2006**, *90*, 939−946.
(45) Bartels, T.; Lankalapalli, R. S.; Bittman, R.; Beyer, K.; Brown, M. F. *J. Am. Chem. Soc.* **2008**, *130*, 14521−14532.
(46) Barenholz, Y. *Subcell Biochem.* **2004**, *37*, 167−215.